Science
AAAS

Ordered and Dynamic Assembly of Single Spliceosomes
Aaron A. Hoskins, *et al.*
Science **331**, 1289 (2011);
DOI: 10.1126/science.1198830

Science (print ISSN 0036-8075; online ISSN 1095-9203) is published weekly, except the last week in December, by the American Association for the Advancement of Science, 1200 New York Avenue NW, Washington, DC 20005.

the use of specific modern groups as analogs for past patterns. Nonetheless, the robustness of our main result suggests that our foraging ancestors evolved a novel social structure that emphasized bilateral kin associations, frequent brother-sister affiliation, important affinal alliances, and coresidence with many unrelated individuals. How this social structure evolved, and how it in turn affected cooperation and cultural capacity—and the role of language in all these features—are key to understanding the emergence of human uniqueness.

References and Notes

1. K. Hill, M. Barton, A. M. Hurtado, *Evol. Anthropol.* **18**, 187 (2009).
2. M. Gurven, *Behav. Brain Sci.* **27**, 543 (2004).
3. P. K. Ivey, G. A. Morelli, E. Z. Tronick, in *Hunter-Gatherer Childhoods: Evolutionary, Developmental and Cultural Perspectives*, B. Hewlett, M. Lamb, Eds. (Aldine de Gruyter, New York, 2005), pp. 191–213.
4. K. Hill, *Hum. Nat.* **13**, 105 (2002).
5. K. Hawkes, J. F. O'Connell, N. G. Jones, H. Alvarez, E. L. Charnov, *Proc. Natl. Acad. Sci. U.S.A.* **95**, 1336 (1998).
6. H. S. Kaplan, K. R. Hill, J. B. Lancaster, A. M. Hurtado, *Evol. Anthropol.* **9**, 156 (2000).
7. S. B. Hrdy, *Mothers and Others* (Belknap, Cambridge, MA, 2009).
8. K. R. Hill, A. M. Hurtado, *Proc. Biol. Sci.* **276**, 3863 (2009).
9. C. F. Camerer, E. Fehr, *Science* **311**, 47 (2006).
10. E. Herrmann, J. Call, M. V. Hernàndez-Lloreda, B. Hare, M. Tomasello, *Science* **317**, 1360 (2007).
11. G. Csibra, *Trends Cogn. Sci.* **11**, 95 (2007).
12. E. Fehr, H. Bernhard, B. Rockenbach, *Nature* **454**, 1079 (2008).
13. J. Henrich *et al.*, *Science* **312**, 1767 (2006).
14. J. B. Silk, *Science* **311**, 1248 (2006).
15. E. Service, *Primitive Social Organization* (Random House, New York, 1962).
16. J. Helm, in *Man the Hunter*, R. B. Lee, I. DeVore, Eds. (Aldine, Chicago, 1968), pp. 118–139.
17. M. Chudek, W. Zhao, J. Henrich, in *Signaling, Commitment, and Emotion*, R. Joyce, K. Sterelny, B. Calcott, Eds. (MIT Press, Cambridge, MA, 2010), pp. 1–24.
18. B. Chapais, *Primeval Kinship: How Pair-Bonding Gave Birth to Human Society* (Harvard Univ. Press, Cambridge, MA, 2008).
19. W. Allen-Arave, M. Gurven, K. R. Hill, *Evol. Hum. Behav.* **29**, 305 (2008).
20. K. Panchanathan, R. Boyd, *Nature* **432**, 499 (2004).
21. R. Boyd, P. J. Richerson, *Proc. Br. Acad.* **88**, 77 (1996).
22. R. Boyd, S. Mathew, *Science* **316**, 1858 (2007).
23. J. Henrich, *Am. Antiq.* **69**, 197 (2004).
24. A. Powell, S. Shennan, M. G. Thomas, *Science* **324**, 1298 (2009).
25. See supporting material on *Science* Online.
26. K. Hill, A. M. Hurtado, *Ache Life History: The Ecology and Demography of a Foraging People* (Aldine, New York, 1996).
27. R. Boyd, P. J. Richerson, *J. Theor. Biol.* **215**, 287 (2002).
28. M. A. Klein, R. Boyd, *Proc. Biol. Sci.* **277**, 2559 (2010).
29. P. Wiessner, *Am. Antiq.* **48**, 253 (1983).
30. S. Mcbrearty, A. S. Brooks, *J. Hum. Evol.* **39**, 453 (2000).

31. We thank each of our study populations for cooperation with data collection, W. Denham for compiling the GCBS database, and B. Chapais, M. Flinn, P. Gardner, M. Gurven, and N. Peterson for discussions.

Supporting Online Material

www.sciencemag.org/cgi/content/full/331/6022/1286/DC1
Materials and Methods
SOM Text
Figs. S1 to S12
Figs. S1 to S3
References

14 October 2010; accepted 18 January 2011
10.1126/science.1199071

Ordered and Dynamic Assembly of Single Spliceosomes

Aaron A. Hoskins,[1,2] Larry J. Friedman,[2] Sarah S. Gallagher,[3]* Daniel J. Crawford,[1,2] Eric G. Anderson,[1] Richard Wombacher,[3]† Nicholas Ramirez,[1]‡ Virginia W. Cornish,[3] Jeff Gelles,[2]§ Melissa J. Moore[1]§

The spliceosome is the complex macromolecular machine responsible for removing introns from precursors to messenger RNAs (pre-mRNAs). We combined yeast genetic engineering, chemical biology, and multiwavelength fluorescence microscopy to follow assembly of single spliceosomes in real time in whole-cell extracts. We find that individual spliceosomal subcomplexes associate with pre-mRNA sequentially via an ordered pathway to yield functional spliceosomes and that association of every subcomplex is reversible. Further, early subcomplex binding events do not fully commit a pre-mRNA to splicing; rather, commitment increases as assembly proceeds. These findings have important implications for the regulation of alternative splicing. This experimental strategy should prove widely useful for mechanistic analysis of other macromolecular machines in environments approaching the complexity of living cells.

The spliceosome is a complex macromolecular machine responsible for removing introns from nascent transcripts via pre-mRNA (precursor to mRNA) splicing (*1*). The spliceosome is composed of five small nuclear RNAs (snRNAs) and ~100 core proteins minimally required for activity in vitro (*2*). The snRNAs and many core proteins are arranged into stable subcomplexes constituting small nuclear ribonucleoprotein particles [U1 and U2 small nuclear ribonucleoproteins (snRNPs) and the U4/U6.U5 tri-snRNP] and the multiprotein Prp19-complex (NTC). Although association of U1 with pre-mRNA can occur in the absence of adenosine triphosphate (ATP), stable association of all other subcomplexes requires ATP hydrolysis. Intron excision occurs after the spliceosome has been fully assembled and activated by additional structural rearrangements (*3*).

Current models of spliceosome assembly, activation, and catalysis generally depict it as an ordered (U1 → U2 → tri-snRNP → NTC → activation → catalysis), one-way process (*3*). Yet deviations from the ordered assembly model have been reported (*4*–*6*), with some studies suggesting that both spliceosome assembly and catalysis are dynamic and reversible (*7*–*9*). None of these studies, however, directly examined the kinetics of subcomplex association with pre-mRNA. We monitored subcomplex dynamics during spliceosome assembly in real time by combining yeast genetic engineering, chemical biology, and a multiwavelength fluorescence technique, colocalization single-molecule spectroscopy (CoSMoS) (*10*).

Labeling spliceosome subcomplexes. We previously established that splicing of single pre-mRNA molecules can be monitored by multiwavelength total internal reflection fluorescence (TIRF) microscopy in the complex environment of *Saccharomyces cerevisiae* whole-cell extract (yeast WCE) (*11*). To enable kinetic analysis of spliceosome assembly, we have now developed methods to introduce fluorophores into individual spliceosomal subcomplexes in WCE. Protein labeling was accomplished using homologous recombination to fuse either a SNAP (an alkylguanine *S*-transferase) (*12*) or an *Escherichia coli* DHFR (dihydrofolate reductase) tag (*13*) onto the C terminus of numerous spliceosomal proteins. These tags enabled us to incorporate bright, photostable organic dyes into the subcomplexes and to avoid the poor photon output and blinking behavior of single fluorescent proteins (*14*). Integration of two orthogonal tags allows for simultaneous monitoring of two different subcomplexes by CoSMoS (Fig. 1). To ensure functionality of the tagged species, we tagged only essential proteins and verified that the resultant strains (table S1) had growth rates and in vitro splicing activities comparable to the parental strain (figs. S1 to S3). By using several selectable markers, we were able to incorporate up to three tags into a single strain. Multiple tags present in the same subcomplex minimized artifacts due to incomplete labeling, photobleaching, and/or long-lived dark-state formation of single fluorophores (*15*).

DHFR tags were labeled by adding excess (20 nM) fluorophore-trimethoprim (TMP) con-

[1]Department of Biochemistry and Molecular Pharmacology, Howard Hughes Medical Institute, University of Massachusetts Medical School, Worcester, MA 01605, USA. [2]Department of Biochemistry, Brandeis University, Waltham, MA 02454, USA. [3]Department of Chemistry, Columbia University, New York, NY 10027, USA.

*Present address: Environmental Protection Agency, Washington, DC 20004, USA.

†Present address: Institute of Pharmacy and Molecular Biotechnology, Heidelberg University, Heidelberg D-69120, Germany.

‡Present address: Department of Molecular and Cellular Biology, Harvard University, Cambridge, MA 02138, USA.

§To whom correspondence should be addressed. E-mail: gelles@brandeis.edu (J.G.); melissa.moore@umassmed.edu (M.J.M.)

jugates (e.g., Cy3-TMP) to WCE. TMP binding to DHFR is noncovalent, but the ternary complex formed between DHFR, TMP, and endogenous NADPH (reduced form of nicotinamide adenine dinucleotide phosphate) (20-30 μM in WCE) is extremely long-lived (*16*). SNAP tags were covalently labeled by incubating WCE with benzylguanine dye conjugates (e.g., SNAP-DY549) and then removing excess dye by gel filtration. SDS–polyacrylamide gel electrophoresis (SDS-PAGE) confirmed labeling specificity (fig. S4A) and efficiency (70 to 90% labeling of functional SNAP tags) (fig. S4B). None of the dye adducts or labeling procedures employed here greatly inhibit splicing in vitro (figs. S2 and S3).

Single-molecule experiments were carried out in WCE containing fluorescently tagged proteins, an O_2 scavenging system, and triplet-state quenchers (*17*). Data were acquired using a TIRF microscope with laser excitation at 488, 532, and 633 nm. Such TIRF experiments detect surface-bound molecules as discrete spots, while fluorescent components in solution remain as diffuse background. To monitor spliceosome assembly, a model pre-mRNA derived from the *rp51a* transcript (*11*, *18*) containing a single fluorophore and 3′ biotin was tethered to a streptavidin-derivatized glass surface at densities of 100 to 250 pre-mRNA molecules per 314 μm^2 field of view (FOV) (Fig. 1). Arrivals and departures of individual spliceosomal subcomplexes were visualized as the appearance and disappearance of fluorescent spots that colocalized with surface-tethered pre-mRNAs.

Subcomplexes accumulate on surface-tethered pre-mRNAs and form functional spliceosomes. The first subcomplex to bind during spliceosome assembly is thought to be U1 snRNP, which interacts with the 5′ splice site (SS). To validate our approach, we monitored U1 association (with DHFR/Cy3-TMP tags on U1 components Snp1 and Prp40) in the presence of ATP with either wild-type (WT) pre-mRNA or a mutant version in which the 5′ SS had been mutated (G/GUAUGU → c/aUAccU). No stable association was observed in the absence of tethered RNA or with the 5′ SS mutant pre-mRNA (Fig. 2, A and B). As expected, U1 spots were present on a surface containing WT pre-mRNA (Fig. 2C). Monitoring of U1 association with WT pre-mRNA over time revealed rapid surface accumulation of U1 signals during the first 5 min (Fig. 2D and movies S1 and S2). In contrast, no time-dependent signal accumulation was observed in the absence of pre-mRNA or with the 5′ SS mutant. Thus, the long-lived signals are dependent both on the presence of pre-mRNA and an intact 5′ SS.

We next compared the kinetics of U1 association with those of U2, tri-snRNP, and the NTC. Binding events for individual subcomplexes were monitored in separate experiments using WCEs containing two DHFR/Cy3-TMP tags on a given subcomplex (table S1). U2 was labeled via the U2-SF3b components Cus1 and Hsh155. Both U1 and U2-SF3b are thought to stably associate with pre-mRNA during assembly and then be expelled before catalytic activation (*2*, *19*). The tri-snRNP and NTC were individually labeled via Brr2 and Snu114 (core U5 components) and Cef1 and Ntc90 (core NTC components). Both U5 and NTC are thought to remain spliceosome-associated throughout activation and catalysis, departing only upon mRNA product release.

As expected, only U1 spots accumulated on WT pre-mRNA in the absence of ATP (Fig. 2E and movie S1). In contrast, all subcomplexes accumulated in the presence of ATP, albeit at different rates (Fig. 2F and movie S2). These rates were consistent with an apparent order of assembly: U1 → U2 → tri-snRNP → NTC. Like U1, accumulation of U2, U5, and NTC was also dependent on an intact 5′ SS (fig. S5A), confirming the specificity of the interactions for a splicing-competent pre-mRNA. Similar results were obtained with the analogous SNAP-tagged strains (fig. S5, B to E).

Although the above results indicated that we could observe subcomplex association with surface-tethered pre-mRNA molecules, they did not reveal what fraction of those pre-mRNAs ultimately spliced. To address this, we combined our previously described Cy3/Alexa647 splicing reporter pre-mRNA (*11*) with extracts in which either U1 or NTC was labeled with SNAP-Atto488 (Fig. 3). In these experiments, disappearance of fluorescence from the Alexa647-labeled intron without loss of the Cy3-labeled exon demonstrates that either the pre-mRNA was spliced and the spliceosome/lariat intron complex departed from the surface-tethered mRNA or that the Alexa647 was photobleached (*11*).

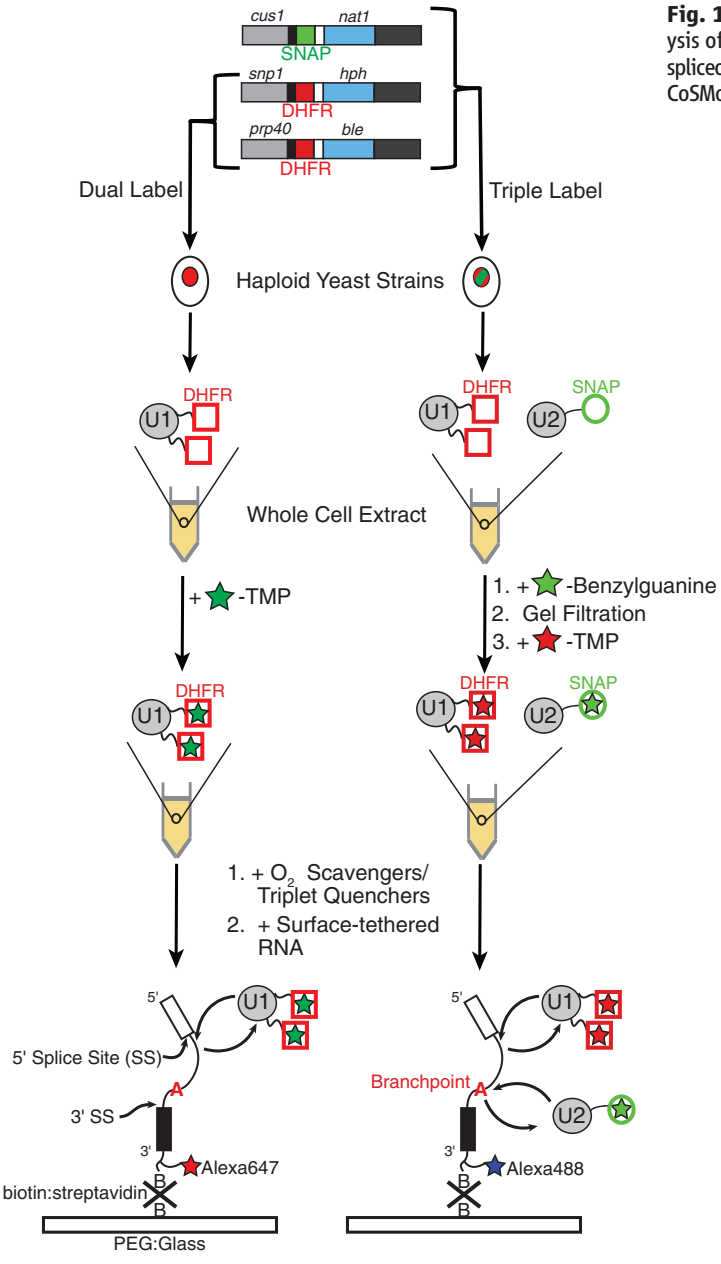

Fig. 1. Preparation and analysis of fluorescently labeled spliceosome subcomplexes by CoSMoS.

Similar to our previous observations (*11*), the extent of intron fluorescence loss was 15 ± 2% (SE) and 18 ± 2% for ATP-containing U1-SNAP and NTC-SNAP extracts, respectively, compared with 4 ± 1% for an inactive no-ATP control (where loss measures photobleaching). These results indicate that active spliceosomes are formed on the surface-linked pre-mRNAs in our labeled extracts. For both U1 and NTC, we could observe numerous pre-mRNAs that both gained the labeled subcomplex and lost intron fluorescence (table S2). Interestingly, only 21 ± 3% of pre-mRNAs that had at least one U1 binding event also lost intron fluorescence. This indicates that interaction with U1 does not absolutely commit a pre-mRNA to splicing. In contrast, roughly half (53 ± 5%) of pre-mRNAs that acquired NTC lost intron fluorescence, suggesting that commitment increases as assembly proceeds. Analysis of individual U1 and NTC binding event lifetimes indicated that pre-mRNAs that ultimately lost their intron signals tended to have U1 lifetimes about twice as long and NTC lifetimes about half as long (fig. S6). One possible explanation is that productive U1 association is stabilized by binding of additional spliceosome assembly factors. Conversely, the shorter NTC lifetime may indicate that properly assembled spliceosomes proceed rapidly through activation, catalysis, and mRNA product release soon after NTC binding.

Order and kinetics of spliceosome assembly. Although the experiments in Fig. 2 can define the population-averaged timing with which different subcomplexes arrive at the pre-mRNA, they do not directly assess the order of subcomplex addition on individual pre-mRNA molecules. Further, the data in Fig. 2 and fig. S5 are composites of subcomplex association and dissociation events, photobleaching, and TMP dye exchange and are additionally complicated by variations in WCE splicing activity. These issues can be resolved by using CoSMoS to simultaneously follow the pre-mRNA association of two spliceosomal subcomplexes in the same WCE. To do so, we used two DHFR/Cy5-TMP tags and a single SNAP DY549 tag to label two subcomplexes (e.g., U1-DHFR and U2-SNAP) with different fluorophores in the same extract (triple-label extracts,

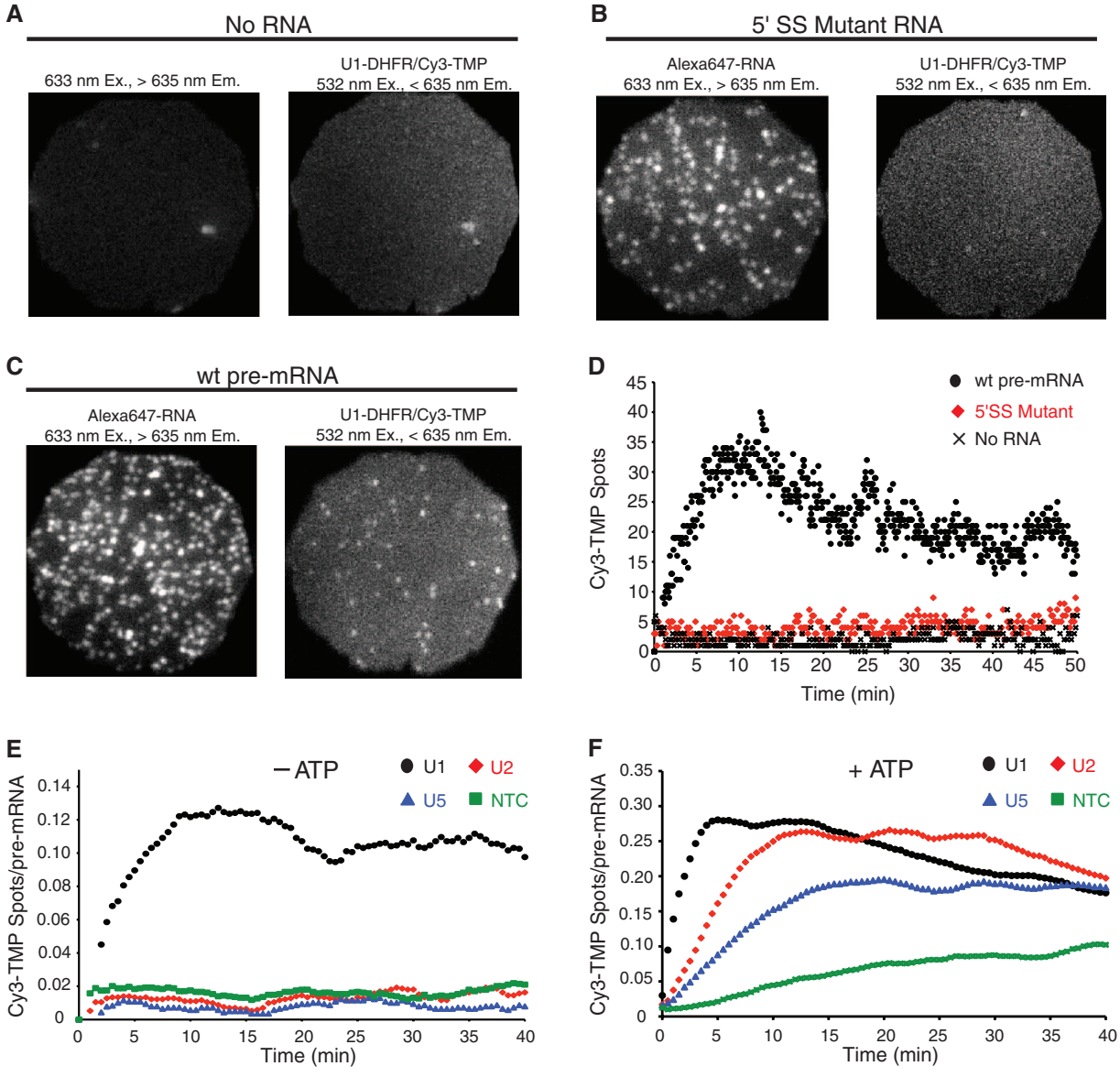

Fig. 2. Individual DHFR-labeled subcomplexes binding to surface-tethered pre-mRNAs. Ex., excitation wavelength; Em., emission wavelength. (**A** to **C**) Images of three FOVs (20 by 20 μm), each at two different emission wavelengths, showing that U1 DHFR Cy3-TMP fluorescence signals (spots) are only observed when WT pre-mRNA is present (C). (**D**) U1 spots versus time in individual FOVs containing RNAs indicated. For WT pre-mRNA, the decrease in spot number after 10 min is due to Cy3-TMP photobleaching in this experiment. Experiments in (A) to (D) contained ATP. (**E** and **F**) Smoothed (9-point moving block averaged) curves of indicated subcomplex spots per pre-mRNA versus time, minus (E) or plus (F) ATP. Each subcomplex was monitored in a different WCE. Data in (**F**) are the average of $n = 4$ replicates.

Fig. 1), and visualized them binding to individual Alexa488-labeled pre-mRNA molecules (Fig. 4, A and B).

As was observed with the individually labeled extracts, when both U1 and U2 were labeled in the same WCE, only U1 colocalized with pre-mRNAs in the absence of ATP, whereas both U1 and U2 colocalized with pre-mRNAs in the presence of ATP (Fig. 4, B and C, and movie S3). When individual pre-mRNA molecules were followed over time, the largest class (49%) (table S3) exhibited at least one discrete onset of U1 fluorescence and at least one discrete onset of U2 fluorescence (Fig. 4D and fig. S7). Other classes exhibited only U1 binding (18%), only U2 binding (6%), or no binding events (27%). These latter subpopulations may arise from the presence of some nonfluorescent subcomplexes in the extract and/or from alternative conformations of the pre-mRNA (*7*, *15*) that prevent spliceosome assembly. U1 and U2 spots persisted for seconds to minutes before disappearing due to either dye photobleaching or subcomplex dissociation. For U1, which was labeled with two DHFR tags, fluorescence typically vanished in one or two discrete steps (96% of events) (table S4). Analogously, for U2, which was labeled with one SNAP tag, fluorescence most often vanished in a single step (88% of events). Thus, only one copy each of U1 and U2 is present at any given time on the majority of pre-mRNAs.

To quantitatively evaluate the U1 and U2 binding order on individual pre-mRNA molecules (Fig. 4D), we calculated t_{U2}-t_{U1}, the difference between the arrival times of the two subcomplexes (*20*). A histogram (Fig. 4E) shows that the overwhelming majority (90%) of these delay times were positive, indicating that U2 binding nearly always followed U1 binding. This conclusion was confirmed by correlation analysis of the absolute binding times (fig. S8), which revealed that even U1 binding events occurring late in the experiment were soon followed by U2 binding. Although U1 and U2 appeared to arrive simultaneously on a small minority (9 out of 223 events) of pre-mRNAs, some of these are likely cases of U1 and U2 arriving in rapid succession separated by a delay that the experimental time resolution (5 to 6 s) was insufficient to resolve (*20*) (table S5). Thus, assembly is highly ordered, with U1 always or almost always binding before U2. Further, >95% of pre-mRNAs that acquire both U1 and U2 acquire them separately rather than as a preformed U1/U2 complex. Consequently, formation of a U1/U2 complex before association with pre-mRNA cannot be a requirement for splicing because the fraction of pre-mRNAs that splice is greater than 5% (table S2).

To examine the ordering of later assembly steps, we used the same methodologies with other triply labeled yeast strains. U2 fluorescence almost always preceded onset of U5 fluorescence (Fig. 4F, fig. S9, and table S6); 97% of the t_{U5}-t_{U2} values were positive (Fig. 4G). Similarly, U5 fluorescence almost always preceded onset of NTC fluorescence (Fig. 4H, fig. S10, and table S7); 91% of the t_{NTC}-t_{U5} delay values were positive (Fig. 4I). In both the U2/U5 and U5/NTC data sets, very few traces (table S5) exhibited apparent simultaneous binding of the subcomplexes, and analysis of all traces suggested that at most one copy each of U5 and NTC were present on the majority of pre-mRNAs (table S4). In sum, our data indicate that when spliceosome assembly is followed on individual RP51A pre-mRNA molecules, the predominant reaction pathway is highly ordered (U1 → U2 → tri-snRNP → NTC). Further, the experiments indicate little or no preassociation for any pair of subcomplexes studied (table S5). As with U1/U2, these data demonstrate that no preassociation of these subcomplexes is required for splicing.

On top of providing information about binding order, the CoSMoS methodology permits measurement of defined kinetic parameters. The arrival times of the first U1 subcomplex on each pre-mRNA and all three time-delay data sets (t_{U2}-t_{U1}, t_{U5}-t_{U2}, and t_{NTC}-t_{U5}) are well fit by single exponential distributions (fig. S11), allowing determination of apparent first-order rate constants (Fig. 5). All four rate constants fall in a narrow range (0.1 to 0.4 min^{-1}), suggesting that no single subcomplex association step predominantly limits the rate of spliceosome assembly on RP51A pre-mRNA.

In addition to arrival times, the triple-label experiments also allowed us to examine the order of subcomplex loss from pre-mRNA. Preliminary analysis revealed that U1 fluorescence tended to be lost before U2 fluorescence, and U2 fluorescence tended to be lost before U5 fluorescence. Only with U5 and NTC did a significant number of pre-mRNAs lose fluorescence from both subcomplexes simultaneously (table S8). These results are consistent with known post-assembly events, including ordered loss of U1 and the SF3b component of U2 during spliceosome activation and subsequent simultaneous loss of U5 and NTC coincident with spliced mRNA release (*2*, *19*). Although additional analyses of photobleaching and Cy5-TMP dye exchange rates will be required to fully interpret these results, they do indicate that subcomplex dissociation coupled to activation and spliceosome disassembly is detectable using this methodology. Definitive analysis of subcomplex dissociation relative to catalysis and intron release awaits future development of more photostable splicing reporters.

We also examined dissociation kinetics of each subcomplex (*20*). In all cases, good fits of

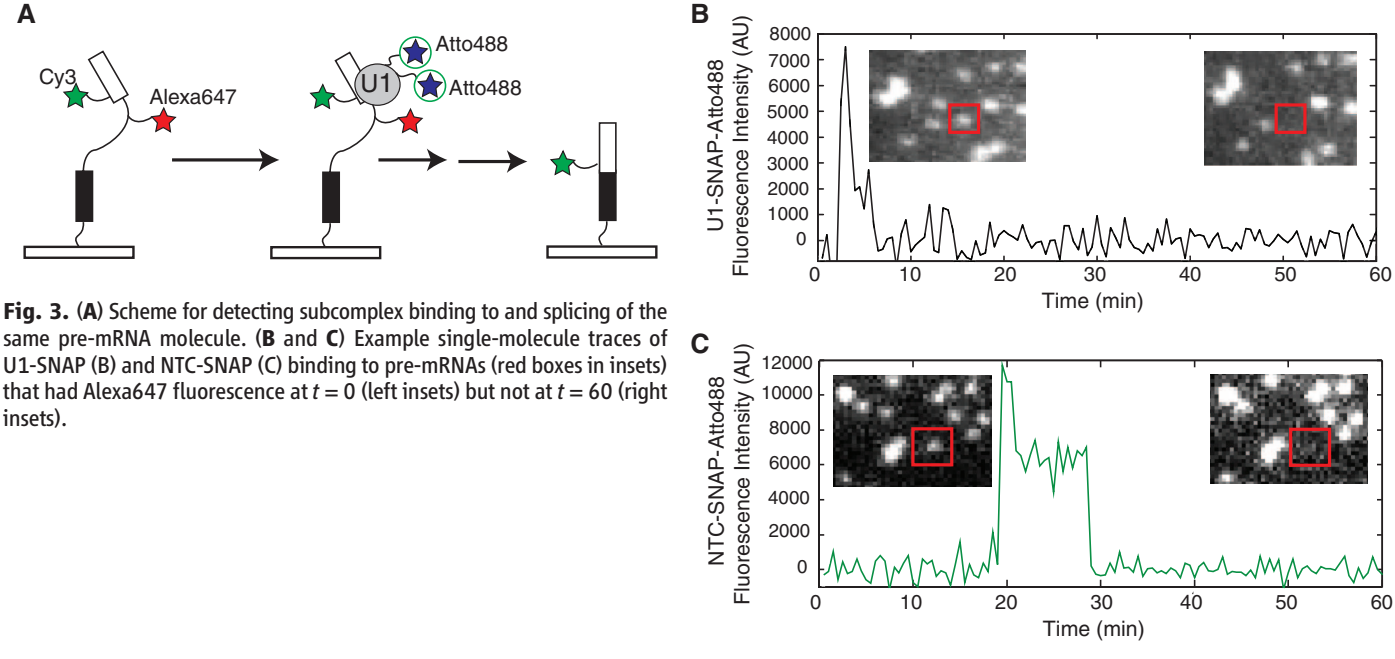

Fig. 3. (**A**) Scheme for detecting subcomplex binding to and splicing of the same pre-mRNA molecule. (**B** and **C**) Example single-molecule traces of U1-SNAP (B) and NTC-SNAP (C) binding to pre-mRNAs (red boxes in insets) that had Alexa647 fluorescence at $t = 0$ (left insets) but not at $t = 60$ (right insets).

dwell-time distributions required a function containing more than one exponential term (fig. S12 and table S9). This presence of both short- (τ_1 < 1 min) and long-lived (τ_2 > 1 min) characteristic dwell times indicates that there is more than one species from which each subcomplex can dissociate. Thus, subcomplex dissociation is more complex than some current models suggest, and there are multiple mechanisms consistent with our data (fig. S13). Elucidation of these mechanisms may be possible by combining CoSMoS with appropriate mutants and inhibitors of assembly.

Pre-mRNAs can engage subcomplexes multiple times. Subsequent to dissociation of a

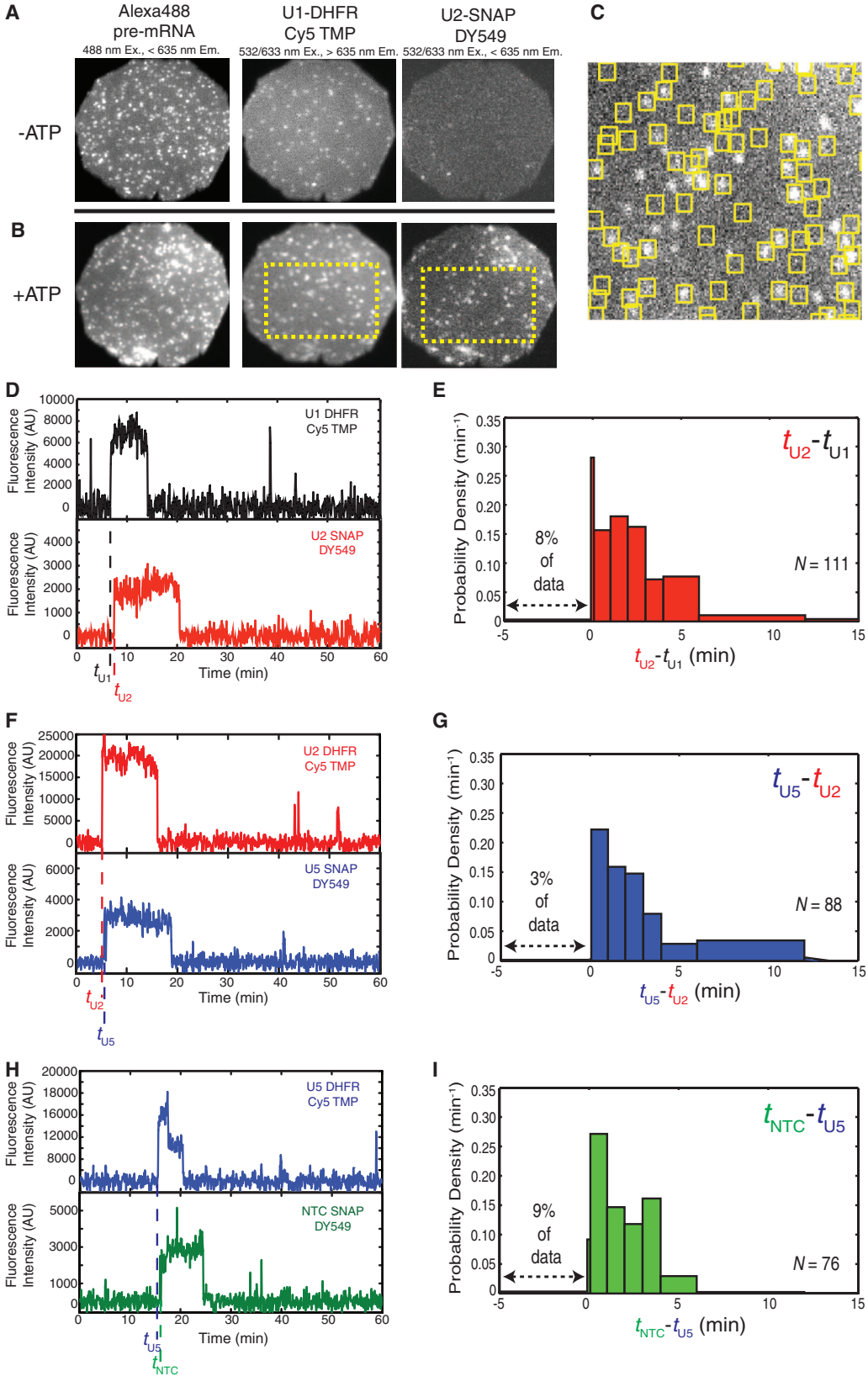

Fig. 4. (**A** and **B**) Images of two FOVs taken at three different wavelengths with triple-label extract to monitor U1-DHFR/Cy5-TMP and U2-SNAP-DY549 association with Alexa488-labeled pre-mRNA, without (A) or with (B) ATP. (**C**) Magnification of dashed area in (B) showing colocalization of U1 (yellow boxes) with U2 (white spots). (**D**) Fluorescence intensity traces showing association of U1 and U2 with an individual pre-mRNA molecule (not shown) in the presence of ATP. Arrival times for each subcomplex (t_{U1} and t_{U2}) are marked. (**E**) Histogram of the delay between subcomplex arrival times (t_{U2}-t_{U1}). (**F** and **H**) Fluorescence intensity traces for U2/U5 (F) and U5/NTC (H) bound to single pre-mRNA molecules (not shown). (**G** and **I**) Histograms of the delays between U2 and U5 binding (G) and U5 and NTC binding (I).

particular subcomplex, many pre-mRNA molecules reacquired a copy of the same subcomplex. On individual pre-mRNAs, U1 often appeared to bind and dissociate repeatedly (Fig. 5A and fig. S14). Use of two covalent SNAP labels on U1 allowed us to verify by photobleaching that the majority of reoccurring U1-SNAP signals resulted from association and dissociation of different U1 molecules (*20*) (fig. S15 and table S10) rather than the blinking of a single molecule (*15*). Further, using the splicing reporter pre-mRNA (Fig. 3), we could observe multiple U1 binding events on pre-mRNAs that spliced (20 ± 7% of pre-mRNAs that lost intron fluorescence acquired multiple U1 signals) (fig. S16). Thus pre-mRNAs that have multiple encounters with U1 are not irreversibly trapped in an inactive state. In the absence of ATP, U1 had a dwell-time distribution nearly identical to that observed in the presence of ATP (fig. S17 and table S9). This suggests that ATP hydrolysis by RNA helicases or other snRNP remodeling enzymes in WCE is not required for U1 dissociation.

A previous study using native PAGE reported two different ATP-independent U1:pre-mRNA complexes: δ_{un} and δ_{commit} (*21*). The more abundant δ_{un} (unstable and uncommitted) did not survive challenge from competitor RNAs, whereas the minor δ_{commit} represented a more stable, challenge-resistant species. Because it could be chased into subsequent steps of the splicing pathway, δ_{commit} is likely the same species as U1-containing commitment complexes (CC1 and/or CC2) (*22*). Our analysis of U1 snRNP dwell times (fig. S12 and table S9) and our observation of U1 dynamics (Fig. 5) provide evidence for at least two types of U1:pre-mRNA complexes with dwell times differing by more than an order of magnitude—an abundant short-lived component likely representing δ_{un} and a longer-lived component likely including CC1 and/or CC2. Consistent with this hypothesis, elimination of the branch site [which is necessary to form CC2 but not CC1 (*18*)] from our transcript (UACUAAC → GUUAGUA) decreased abundance of the longer-lived component but did not abolish it (fig. S18 and table S9). Thus, the long-lived component must contain species in addition to CC2.

We have also observed multiple arrivals and departures of U2, U5, and the NTC on individual

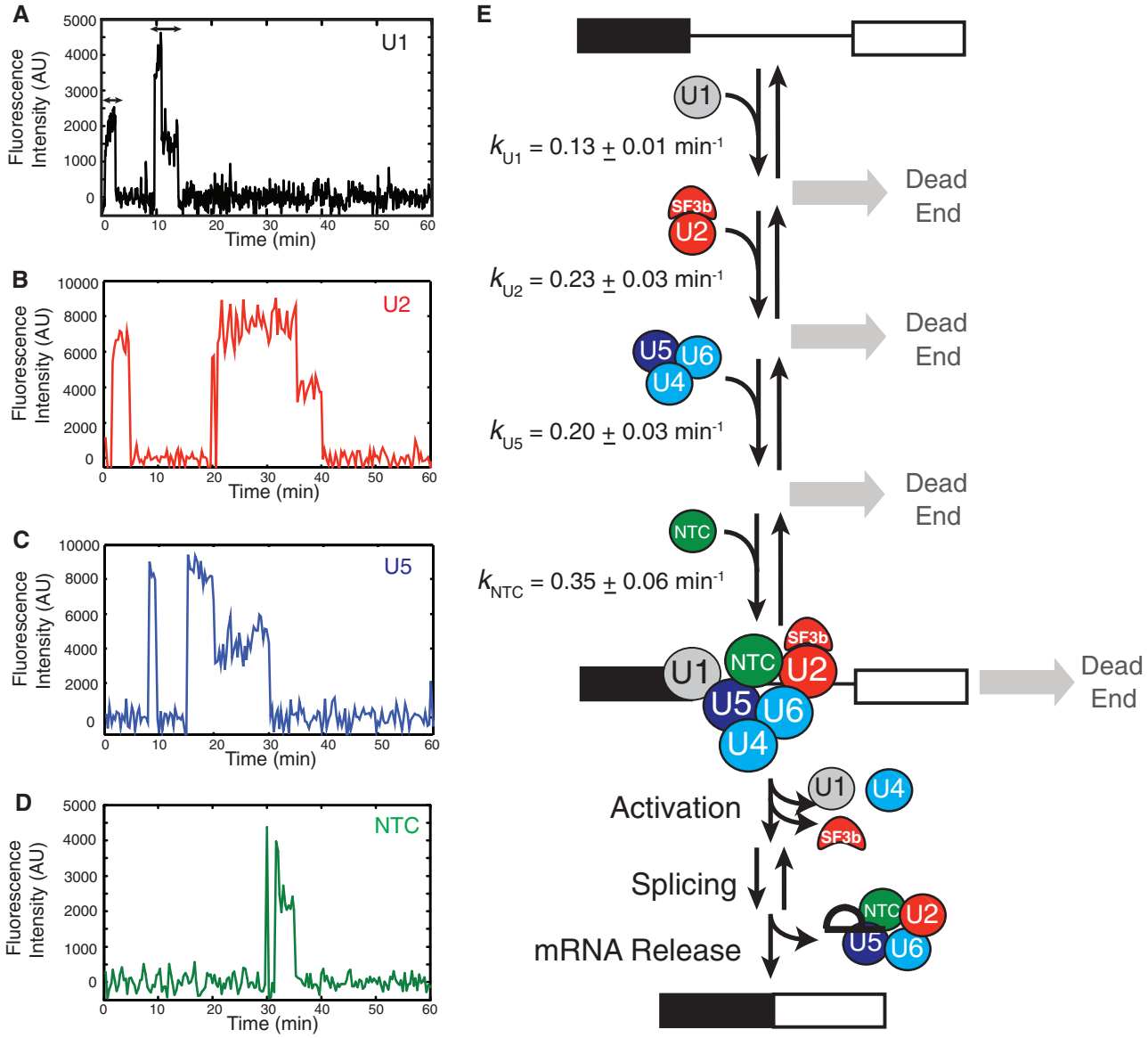

Fig. 5. (**A** to **D**) Single-molecule traces of SNAP-DY549–labeled subcomplexes binding and dissociating multiple times from individual pre-mRNA molecules (not shown) in the presence of ATP. Arrows indicate durations of two U1 binding events (dwell times) used to analyze U1 lifetimes. (**E**) Kinetic scheme for spliceosome assembly and splicing of RP51A pre-mRNA. Our results provide evidence for reversible binding of all of the major subcomplexes (backward arrows), whereas others have provided evidence for reversibility of splicing chemistry (*8*). There is as yet no evidence for reversibility of the activation step before splicing or mRNA release.

pre-mRNAs (Fig. 5, B to D, and figs. S14 and S19). As seen with U1, multiple NTC binding events could be detected on the splicing reporter pre-mRNA (4 ± 2% of pre-mRNAs both lost their intron signal and acquired NTC more than once) (fig. S16). The number of binding events observed per pre-mRNA molecule was dependent on the subcomplex being studied. U1 exhibited by far the largest number of binding events, with the number of events systematically decreasing for each successive subcomplex in the pathway (fig. S20). This suggests that at each step of subcomplex addition, some fraction of the pre-mRNA molecules are lost to side pathways that do not lead to productive splicing (Fig. 5E).

Discussion. Taken together, the data from this real-time kinetic analysis of spliceosome assembly are consistent with existing models and lead to new insights. Spliceosome assembly on the RP51A substrate is highly ordered (U1 → U2 → tri-snRNP → NTC), and pre-association of the subcomplexes is not required for splicing. Although no single step appears to irreversibly commit this pre-mRNA to splicing, commitment increases as spliceosome assembly proceeds. Further, spliceosome assembly on this pre-mRNA is kinetically efficient, with no single subcomplex binding step predominantly restricting the overall rate. Finally, we have directly observed multiple binding events for all subcomplexes, demonstrating that subcomplex binding is reversible. Together, these findings have important implications for the regulation of alternative splicing. If spliceosome assembly is reversible and no single assembly step irreversibly commits a particular pair of splice sites to splicing, then alternative splice site choice can potentially be regulated at any stage of assembly. This hypothesis is bolstered by observations that some regulation of alternative splicing apparently occurs at late stages of assembly (*23*, *24*).

By making possible kinetic analysis of spliceosome assembly in whole-cell extracts, this work opens the door to answering fundamental questions concerning the mechanisms of pre-mRNA splicing. The combination of CoSMoS with chemical and genetic tools is a powerful approach for elucidating the mechanisms of complex biological processes, even when those processes can only be studied in cell extracts. These methods should prove broadly useful for analyzing many other complex macromolecular machines.

References and Notes

1. T. W. Nilsen, *Bioessays* **25**, 1147 (2003).
2. P. Fabrizio *et al.*, *Mol. Cell* **36**, 593 (2009).
3. M. C. Wahl, C. L. Will, R. Lührmann, *Cell* **136**, 701 (2009).
4. S. W. Stevens *et al.*, *Mol. Cell* **9**, 31 (2002).
5. Y. Z. Xu *et al.*, *EMBO J.* **23**, 376 (2004).
6. M. Schneider *et al.*, *Mol. Cell* **38**, 223 (2010).
7. J. Abelson *et al.*, *Nat. Struct. Mol. Biol.* **17**, 504 (2010).
8. C. K. Tseng, S. C. Cheng, *Science* **320**, 1782 (2008).
9. L. Liu, C. C. Query, M. M. Konarska, *Nat. Struct. Mol. Biol.* **14**, 519 (2007).
10. L. J. Friedman, J. Chung, J. Gelles, *Biophys. J.* **91**, 1023 (2006).
11. D. J. Crawford, A. A. Hoskins, L. J. Friedman, J. Gelles, M. J. Moore, *RNA* **14**, 170 (2008).
12. A. Juillerat *et al.*, *Chem. Biol.* **10**, 313 (2003).
13. L. W. Miller, Y. Cai, M. P. Sheetz, V. W. Cornish, *Nat. Methods* **2**, 255 (2005).
14. R. M. Dickson, A. B. Cubitt, R. Y. Tsien, W. E. Moerner, *Nature* **388**, 355 (1997).
15. I. Rasnik, S. A. McKinney, T. Ha, *Nat. Methods* **3**, 891 (2006).
16. S. M. Dunn, R. W. King, *Biochemistry* **19**, 766 (1980).
17. R. Dave, D. S. Terry, J. B. Munro, S. C. Blanchard, *Biophys. J.* **96**, 2371 (2009).
18. B. Séraphin, M. Rosbash, *EMBO J.* **10**, 1209 (1991).
19. R. M. Lardelli, J. X. Thompson, J. R. Yates 3rd, S. W. Stevens, *RNA* **16**, 516 (2010).
20. Materials and methods are available as supporting material on *Science* Online.
21. S. W. Ruby, *J. Biol. Chem.* **272**, 17333 (1997).
22. P. Legrain, B. Seraphin, M. Rosbash, *Mol. Cell. Biol.* **8**, 3755 (1988).
23. M. Chen, J. L. Manley, *Nat. Rev. Mol. Cell Biol.* **10**, 741 (2009).
24. S. Bonnal *et al.*, *Mol. Cell* **32**, 81 (2008).

25. We thank J. Chung, A. Okonechnikov, J. Yan, J. Haber, S. Lovett, I. Correa, M.-Q. Xu, Z. Chen, and B. Smith for helpful discussions and assistance. This work was supported by NIH RO1s GM043369 (J.G.), GM81648 (J.G.), GM053007 (M.J.M), GM54469 (V.W.C.), RC1 GM091804 (V.W.C), National Research Service Award fellowship GM079971 (A.A.H.), and K99/R00 GM086471 (A.A.H.). D.J.C., S.S.G., and R.W were supported by NIH training grant GM759628, a National Defense Science and Engineering Graduate fellowship, and a Deutscher Akademischer Austausch Dienst fellowship, respectively. M.J.M. is a Howard Hughes Medical Institute investigator. V.W.C. holds patents on the TMP-tag technology, and the technology is licensed and commercialized by Active Motif.

Supporting Online Information

www.sciencemag.org/cgi/content/full/331/6022/1289/DC1
Materials and Methods
Figs. S1 to S21
Scheme S1
Tables S1 to S12
Movies S1 to S3
References

7 October 2010; accepted 28 January 2011
10.1126/science.1198830

Organic Aerosol Formation Downwind from the Deepwater Horizon Oil Spill

J. A. de Gouw,[1,2]* A. M. Middlebrook,[1] C. Warneke,[1,2] R. Ahmadov,[1,2] E. L. Atlas,[3] R. Bahreini,[1,2] D. R. Blake,[4] C. A. Brock,[1] J. Brioude,[1,2] D. W. Fahey,[1] F. C. Fehsenfeld,[1,2] J. S. Holloway,[1,2] M. Le Henaff,[3] R. A. Lueb,[5] S. A. McKeen,[1,2] J. F. Meagher,[1] D. M. Murphy,[1] C. Paris,[3] D. D. Parrish,[1] A. E. Perring,[1,2] I. B. Pollack,[1,2] A. R. Ravishankara,[1] A. L. Robinson,[6] T. B. Ryerson,[1] J. P. Schwarz,[1,2] J. R. Spackman,[1,2] A. Srinivasan,[3] L. A. Watts[1,2]

A large fraction of atmospheric aerosols are derived from organic compounds with various volatilities. A National Oceanic and Atmospheric Administration (NOAA) WP-3D research aircraft made airborne measurements of the gaseous and aerosol composition of air over the Deepwater Horizon (DWH) oil spill in the Gulf of Mexico that occurred from April to August 2010. A narrow plume of hydrocarbons was observed downwind of DWH that is attributed to the evaporation of fresh oil on the sea surface. A much wider plume with high concentrations of organic aerosol (>25 micrograms per cubic meter) was attributed to the formation of secondary organic aerosol (SOA) from unmeasured, less volatile hydrocarbons that were emitted from a wider area around DWH. These observations provide direct and compelling evidence for the importance of formation of SOA from less volatile hydrocarbons.

On 20 April 2010, the Deepwater Horizon (DWH) offshore drilling unit exploded, causing the riser pipe to rupture and crude oil to flow into the Gulf of Mexico from a depth of ~1500 m. The oil leak rate was estimated to be 68,000 barrels per day (*1*), and much of that oil accumulated on the sea surface. A NOAA WP-3D research aircraft equipped with a large number of instruments to characterize trace gases and aerosols (*2*) performed two flights near DWH on 8 and 10 June to explore the atmospheric impacts of the spilled oil and of the cleanup activities near DWH. This report discusses one of those impacts: the formation of large concentrations of secondary organic aerosol (SOA) observed downwind from the oil spill. These findings have implications for our general understanding of organic aerosol, which is a large but poorly understood class of atmospheric aerosol

[1]Chemical Sciences Division, Earth System Research Laboratory, National Oceanic and Atmospheric Administration, Boulder, CO 80305, USA. [2]Cooperative Institute for Research in Environmental Sciences, University of Colorado, Boulder, CO 80309, USA. [3]Rosenstiel School of Marine and Atmospheric Science, University of Miami, Miami, FL 33149, USA. [4]Department of Chemistry, University of California, Irvine, CA 92697, USA. [5]Atmospheric Chemistry Division, Earth System Laboratory, National Center for Atmospheric Research, Boulder, CO 80301, USA. [6]Center for Atmospheric Particle Studies, Carnegie Mellon University, Pittsburgh, PA 15213, USA.

*To whom correspondence should be addressed. E-mail: joost.degouw@noaa.gov